Three-Dimensional Numerical Simulations of Viscoelastic Phase Separation: Morphological Characteristics

Takeaki Araki and Hajime Tanaka*

Institute of Industrial Science, University of Tokyo, Meguro-ku, Tokyo 153-8505, Japan

Received September 11, 2000; Revised Manuscript Received December 8, 2000

ABSTRACT: We have studied the characteristic features of viscoelastic phase separation in three dimensions by using numerical simulations, focusing on the morphological development. The Langevin-type equations of a two-fluid model, which includes both bulk and shear viscoelastic stresses, are solved numerically. The origin of phase inversion is discussed on the basis of a simple consideration on the symmetry of the "effective" phase diagram, and the importance of the bulk stress on this phenomenon is addressed. The roles of bulk and shear stresses are clarified by comparing simulation results for cases with and without each stress. We analyzed the temporal change in the structure factor and found that the structure factors cannot be scaled, and thus, the dynamical scaling law does not hold at all for viscoelastic phase separation. We also studied the geometrical characteristics such as the mean and Gaussian curvatures and the Euler characteristic of the interface, to characterize the topological features of viscoelastic phase separation. The results also unambiguously indicated the absence of the self-similarity, which is the central concept of the late-stage pattern evolution in conventional phase separation. The topological change accompanied by phase inversion was successfully characterized by the curvature of domain interface and the Euler charactristic. Our study indicated the advantage of the real-space analysis over the q (wavenumber)-space one in the topological characterization.

I. Introduction

Phase-separation phenomena are widely observed in various kinds of binary mixtures including metals, semiconductors, simple liquids, and complex fluids such as polymers, surfactants, colloids, and biological materials.[1] Phase separation in polymer solutions and polymer mixtures are thought to be the same as that in classical fluid mixtures (model H in the Hohenberg−Halperin notation[2]).[1,3] This is true when the difference in viscoelastic properties between two coexisting phases is small, e.g., near a critical point, for a mixture of polymers having similar molecular weights and glass-transition temperatures or for a solution of polymer with low molecular weight. In contrast to this common belief, one of us recently found a new type of phase-separation behavior in polymer solutions. It is named "viscoelastic phase separation"[4−6] since viscoelastic effects play a crucial role in pattern evolution. It was demonstrated that this unusual phenomenon is caused by strong "dynamic asymmetry" between the two components of a mixture. Actually, viscoelastic phase separation is also observed in polymer blends, one of whose components is close to its glass transition temperature.[7] This indicates that dynamic asymmetry is the only requirement for viscoelastic phase separation and suggests the universal nature of viscoelastic phase separation. For example, it is expected that viscoelastic phase separation will also be observed in colloidal suspensions and emulsions.[8,9]

Viscoelastic phase separation is characterized by unusual phase-separation behaviors.[9] They include the moving droplet phase, which coarsens unusually slowly, and the phase-inversion phenomena in the late-stage of phase separation.[6] Such behaviors are never observed in conventional phase separation. In particular, networklike phase separation is interesting since a minority phase can transiently form a continuous phase there. This phenomenon has a technological importance, since it enables us to intentionally form the continuous network structure of a minority phase. It proceeds as follows: (i) Just after a temperature quench, a transient gel is formed. (ii) The solvent-rich phase, which is thermodynamically a majority phase, is selectively nucleated after some incubation period. (ii) The polymer-rich phase shrinks as chemical gel shrinks. (iii) In this process, the networklike structure of the polymer-rich phase is transiently formed. (iv) In the final stage, the network structure relaxes to circular isolated domains. In this way, phase inversion takes place in this phase separation. It is obvious that there is no self-similarity and no dynamic scaling for the pattern evolution of viscoelastic phase separation.

It was demonstrated[9,10] that viscoelastic phase separation is well described by a two-fluid model[11−15] by including the bulk stress. The bulk stress was introduced into the rheological constitutive equation[9,10] to express the formation of a transient gel right after the initiation of phase separation. It was also shown[9,10] that the viscoelastic model is a quite universal model of phase separation in isotropic systems, which contains a fluid model (model H) and a solid model(model B) as a special case. The initial stage of viscoelastic phase separation was theoretically studied by Onuki and Taniguchi[16] and by Kumaran and Frederickson.[17] To study the late stage of phase separation, however, we need to perform numerical simulations. Sappelt and Jäckle[18] and Ahluwalia[19] made the coarse-grained simulations, which are based on a "solid model" (model B). These models assume the asymmetry of the diffusion coefficient to suppress the concentration fluctuations in polymer-rich phase selectively. The results reproduced the selective nucleation of the solvent-rich phase and the phase inversion in the late stage. However, this method neglects the fluid nature of a mixture, or viscoelastic effects. Thus, viscoelastic stresses play no roles in this type of model.[9] Taniguchi and Onuki[20] and

10.1021/ma001569n CCC: $20.00
Published on Web 02/10/2001

we[21] simulated viscoelastic phase separation based on a "two-fluid" model, in which the coupling between concentration diffusion and viscoelastic stress are considered.[15,22,23] In these studies, it was shown that viscoelastic stresses play important roles in the formation of the networklike structure. It should be noted that the similar simulations were made also by Sagui et al.[24] and Okuzono.[25] Bhattacharya et al. and Liu et al.[26] made molecular dynamics simulations, which take into account the connectivity of polymer chains. The results indicated the importance of the entanglements of polymers in the formation and the breakup of the networklike structure on a mesoscopic level.

In our previous numerical simulations,[21] we newly introduced the bulk stress into a two-fluid model, which is known to be important in the volume shrinking of gels,[27] in addition to the shear stress. Our results reproduced all the essential features of viscoelastic phase separation observed experimentally. This indicates the importance of bulk stress, which is directly coupled to the concentration field and suppresses the concentration fluctuations in the polymer-rich phase selectively. The roles of bulk and shear stresses in pattern evolution were revealed. We stress that the bulk stress is caused by the formation of a transient gel, which is due to the asymmetry in elementary dynamics between the two components of a mixture.[9,10,28,29]

Most previous simulations have so far been limited to two dimensions. To gain an insight into the topological characteristics of patterns, we need to perform three-dimensional simulations. In this paper, thus, we numerically simulate viscoelastic phase separation in three dimensions to answer the following questions: (i) How is the networklike structure characterized in 3D? (ii) How can phase inversion be described in terms of topological characteristics? (iii) Do the roles of the shear and bulk stresses depend on the dimensionality or not?

In section II, we review the viscoelastic model based on a two-fluid model. In section III, we explain the details of numerical simulations. In section IV, we discuss the mechanism of the phase inversion. In section V, we show the results and discuss them. Finally we summarize our work.

II. Viscoelastic Model: Two-fluid Model

Here we describe the Langevin-type equations of viscoelastic phase separation of polymer solutions used in this study. They are based on a "two-fluid" model of a mixture of polymer p and solvent s.[15,21] Let $\vec{v}_p$ and $\vec{v}_s$ be the average velocities of polymer and solvent, respectively, and $\phi(\vec{r},t)$ be the concentration of polymer at a point $\vec{r}$ and time t. We employ the Flory−Huggins-type mixing free energy functional given by

$$F_{mix}\{\phi,T\} = \int d\vec{r}\{f_{FH}(\phi,T) + C|\vec{\nabla}\phi|^2/2\} \quad (1)$$

$$f_{FH}(\phi,T) = k_B T\{(1/N_p)\phi \ln \phi + (1-\phi)\ln(1-\phi) + \chi(T)\phi(1-\phi)\} \quad (2)$$

Here k_B is Boltzmann's constant, T is the temperature, N_p is the degree of polymerization, and χ is the Flory−Huggins interaction parameter. In this study, however, we set $N_p = 1$ and neglect the ϕ dependence of the coefficient of the gradient term C in order to pick up the pure effects of viscoelastic stresses on the phase-separation kinetics.

The kinetic equations are given by

$$\frac{\partial\phi}{\partial t} = -\vec{\nabla}\cdot(\phi\vec{v}_p) + \theta \quad (3)$$

$$\vec{v}_p - \vec{v}_s = -\frac{1-\phi}{\zeta}[\vec{\nabla}\cdot\mathbf{\Pi} - \vec{\nabla}\cdot\boldsymbol{\sigma}] \quad (4)$$

$$\zeta_0\frac{\partial\vec{v}}{\partial t} \cong -\vec{\nabla}\cdot\mathbf{\Pi} + \vec{\nabla}\cdot\boldsymbol{\sigma} - \vec{\nabla}\tilde{p} + \eta_s\nabla^2\vec{v} \quad (5)$$

where θ represents the coarse-grained thermal concentration fluctuations, ζ is a friction constant between polymer and solvent, and η_s is the viscosity of a solvent. Here $\vec{v}$ is the averaged velocity field of the solution and is given by $\vec{v} = \phi\vec{v}_p + (1-\phi)\vec{v}_s$. $\tilde{p}$ is a part of the pressure, which is determined to satisfy the following incompressible condition:

$$\vec{\nabla}\cdot\vec{v} = 0 \quad (6)$$

For simplicity, we assume that both polymer and solvent have the same density ρ_0. $\mathbf{\Pi}$ is a thermodynamical osmotic stress tensor and is related to the mixing free energy F_{mix} as

$$\vec{\nabla}\cdot\mathbf{\Pi} = \phi\vec{\nabla}\frac{\delta F_{mix}}{\delta\phi} = \phi\vec{\nabla}\left(\frac{\partial f_{FH}}{\partial\phi} - C\nabla^2\phi\right) \quad (7)$$

The temporal change of ϕ and $\vec{v}_p$ are slow in our system so that the inertia term in eq 5 can be neglected. Thus, we assume

$$\zeta_0\frac{\partial\vec{v}}{\partial t} \approx 0 \quad (8)$$

Under the incompressible (eq 6) and quasi-stationary (eq 8) conditions, eq 5 reduces to

$$\vec{v}(\vec{r}) = \int d\vec{r}'\boldsymbol{T}(\vec{r}-\vec{r}')\cdot\{\vec{\nabla}\cdot(-\mathbf{\Pi}(\vec{r}') + \boldsymbol{\sigma}(\vec{r}'))\} \quad (9)$$

Here $\boldsymbol{T}(\vec{r})$ is the Oseen tensor given by

$$\boldsymbol{T}(\vec{r}) = \frac{1}{8\pi\eta_s r}\left[\boldsymbol{I} + \frac{\vec{r}\vec{r}}{r^2}\right]$$

Thus, $\vec{v}_p$ is obtained from eqs 4 and 9 as

$$\vec{v}_p(\vec{r}) = \frac{(1-\phi(\vec{r}))^2}{\zeta}\vec{\nabla}\cdot\{-\mathbf{\Pi}(\vec{r}') + \boldsymbol{\sigma}(\vec{r}')\} + \int d\vec{r}'\boldsymbol{T}(\vec{r}-\vec{r}')\cdot\vec{\nabla}\cdot\{-\mathbf{\Pi}(\vec{r}') + \boldsymbol{\sigma}(\vec{r}')\} \quad (10)$$

$\boldsymbol{\sigma}$ is the viscoelastic stress tensor, which should be supported solely by polymers and not by solvent molecules. Thus, the associated deformation can be expressed only by $\vec{v}_p$. Although only the shear part of viscoelastic stress was considered in the original two-fluid model[15] for polymer solutions, we newly introduced the bulk stress in addition to the shear one[9,10,28] and demonstrated[21] that the bulk part of viscoelastic stress plays an important role in the phase-separation process as in the case of the volume phase transition of gels. Thus, the total stress is given by

$$\boldsymbol{\sigma} = \boldsymbol{\sigma}_B + \boldsymbol{\sigma}_S \quad (11)$$

Here the suffixes B and S mean the bulk and shear stresses, respectively. Note that the bulk stress $\boldsymbol{\sigma}_B$ stems from the motion of polymers itself. Thus, it intrinsically has the mechanical origin. In other words, $\boldsymbol{\sigma}_B$ cannot

be included in **II**. For simplicity, we assume that viscoelastic relaxation of each stress is single relaxational (or Debye-type). For such a case, it is known that the shear stress obeys the following upper-convective Maxwell equation

$$\frac{D}{Dt}\boldsymbol{\sigma}_S = \boldsymbol{\sigma}_S \cdot \vec{\nabla} v_p + (\vec{\nabla} v_p)^T \cdot \boldsymbol{\sigma}_S - \frac{1}{\tau_S(\phi)}\boldsymbol{\sigma}_S + G_S(\phi)\{\vec{\nabla} v_p + (\vec{\nabla} v_p)^T\} \quad (12)$$

where

$$\frac{D}{Dt} = \frac{\partial}{\partial t} + \vec{v}_p \cdot \vec{\nabla}$$

τ_S and G_S are a relaxation time and a modulus of the shear stress, respectively. Note that $(\vec{\nabla} v_p)_{ij} = \partial_i v_{pj}$. Since the shear stress is a traceless tensor, we calculate the final form of shear stress as $\boldsymbol{\sigma}_S^f = \boldsymbol{\sigma}_S - (1/d)\mathrm{Tr}\boldsymbol{\sigma}_S \boldsymbol{I}$, where $\boldsymbol{I}$ is a unit tensor and d is the space dimensionality. Hereafter, the shear stress $\boldsymbol{\sigma}_S$ means this final form $\boldsymbol{\sigma}_S^f$. Since the bulk stress is isotropic, on the other hand, it can be expressed by a scalar variable, namely, $\mathrm{Tr}\boldsymbol{\sigma}_B$. Thus, the bulk stress obeys the following equations:

$$\frac{D}{Dt}\tilde{\sigma} = -\frac{1}{\tau_B(\phi)}\tilde{\sigma} + G_B(\phi)\vec{\nabla} \cdot \vec{v}_p \quad (13)$$

$$\boldsymbol{\sigma}_B = \tilde{\sigma}\boldsymbol{I} \quad (14)$$

Here, τ_B and G_B are a relaxation time and a modulus of the bulk stress, respectively. Note that $\tilde{\sigma} = (1/d)\mathrm{Tr}\boldsymbol{\sigma}_B$.

For the shear mode, some theories, such as the reptation model[30] and the scaling relation,[31] predict the behaviors of τ_S and G_S. They are known to depend on the concentration field ϕ in good and/or Θ solvents as follows:[32]

$$G_S \propto \phi^{\gamma} \quad (15)$$

$$\tau_S \propto \phi^{\alpha} \quad (16)$$

However, the values of γ and α in a poor solvent condition, where phase separation occurs, are not available. In our study, thus, we assume that $\gamma = 2$ and $\alpha = 2$ for simplicity.

It is quite difficult to make any theoretical prediction on the bulk stress. From both experimental observation and physical consideration, however, we argue that a polymer solution transiently behaves as a gel just after the temperature quench and the destruction of this transient gel is the process of the selective nucleation of a solvent-rich phase.[9] Thus, we express the formation and relaxation of a transient gel by using the following form for the bulk stress

$$G_B \propto \Theta(\phi - \phi_0) \quad (17)$$

$$\tau_B \propto \phi^2 \quad (18)$$

where Θ is a step function. The physical relevance of the above form of the bulk stress was discussed in refs 8−10.

III. Numerical Simulations

The basic equations described in section II are numerically solved by discretizing time and space in three dimensions using the periodic boundary condition. A simulated space size is $64 \times 64 \times 64$. To calculate eq 3, we employ the explicit Euler method and set a grid size to $\Delta x = 1$ and a time increment to $\Delta t = 0.01$. We solve eq 9 using a fast Fourier transformation method.[33] To reduce the computational cost, we solve the time development equations except for eq 9 without updating velocity field by skipping N_{skip} cycles. In this study, we set $N_{skip} = 10$. We confirm the absence of any meaningful differences between the simulations with $N_{skip} = 10$ and those with $N_{skip} = 1$.

Stress tensors of shear (eq 12) and bulk (eq 13) modes are calculated by using the following relations:[21]

$$\boldsymbol{\sigma}_S(\vec{r}, t + \Delta t) = \boldsymbol{\sigma}_S(\vec{r}, t)\exp\left(-\frac{\Delta t}{\tau_S}\right) + [-\vec{v}_p \cdot \vec{\nabla}\sigma_S + \boldsymbol{\sigma}_S \cdot \vec{\nabla} v_p + (\vec{\nabla} v_p)^T \cdot \boldsymbol{\sigma}_S + G_S\{\vec{\nabla} v_p + (\vec{\nabla} v_p)^T\}]\Delta t \quad (19)$$

$$\tilde{\sigma}(\vec{r}, t + \Delta t) = \tilde{\sigma}(\vec{r}, t)\exp\left(-\frac{\Delta t}{\tau_B}\right) + [-\vec{v}_p \cdot \vec{\nabla}\sigma + G_B\vec{\nabla} \cdot \vec{v}_p]\Delta t \quad (20)$$

This method coincides with the usual Euler method up to the order Δt, and has a significant advantage over it on the following point. This method is free from numerical instabilities even for $\Delta t \geq \tau_B$ and/or τ_S. In other words, it allows us to treat a very wide range of the stress relaxation time without suffering from the instability problems.

In this study, we set the parameters as $k_B T = 1.3$, $\chi = 2.7$, $C = 1$, $\zeta = 0.1$, and $\eta_s = 0.1$. This set of parameters was chosen so that the coarsening behavior without viscoelastic stresses should coincide with that of the fully scaled time-dependent Ginzburg−Landau equation with hydrodynamic interactions (model H).[34] We introduce the Gaussian random noises of ϕ with the intensity $\delta\phi = 0.1$ around the averaged polymer concentration $\phi_0 = 0.3$ at $t = 0$ under the constraint of $0 < \phi < 1$. For these parameters, the equilibrium concentrations ϕ_e are nearly 0.107 and 0.893, and the final volume fraction of polymer-rich phase is about 24.5%. It should be noted that for this volume fraction a droplet structure should be observed in usual fluid phase separation (see the following case b). We study cases of phase separation with both bulk and shear stresses (a), without any stress (b), with only shear stress (c), with only bulk stress (d), and with both stresses but with a longer shear relaxation time (e). The parameters we used are listed in Table 1. We also performed other simulations (f and g), in which we used the step-function form also for the shear modulus (eq 17) instead of the analytical form (eq 15), to study how the shear stress affects the pattern evolution in the early stage of phase separation. The parameter used and the roles of stresses are summarized in Table 1.

IV. Effective Phase Diagram and Roles of Bulk Stress

It is known that the external shear flow affects the position of the spinodal line of a polymer solution.[12−15] There are intensive studies on the shear-induced phase separation in polymer systems. In this problem, the bulk stress does not play any important role, since it is not coupled with shear flow. The concept of the bulk stress is newly introduced to express the unique mechanical properties of a transient gel.[10,28] So it is meaningful to

reveal the roles of shear and bulk stresses in the early-stage phase separation. Here we reconsider the concept of the "effective" phase diagram and dynamic symmetry line[6] on a more quantitative basis.

In the early stage of phase separation, the viscoelastic stress can be approximated from eqs 12 and 13 as

$$\sigma_{ij} = \int_0^t dt' \Big[G_B(\phi) e^{-(t-t')/\tau_B(\phi)} \partial_k v_{pk} \delta_{ij} + G_S(\phi) e^{-(t-t')/\tau_S(\phi)} \Big\{ \partial_i v_{pj} + \partial_j v_{pi} - \frac{2}{d} \partial_k v_{pk} \delta_{ij} \Big\} \Big] \quad (21)$$

When the temporal change of $\vec{v}_p$ is faster than the relaxation time, eq 21 reduces to

$$\sigma_{ij} = G_B(\phi) \partial_k u_{pk} \delta_{ij} + G_S(\phi) \Big\{ \partial_i u_{pj} + \partial_j u_{pi} - \frac{2}{d} \partial_k u_{pk} \delta_{ij} \Big\} \quad (22)$$

where $\vec{u}_p = \int_0^t dt' \, \vec{v}_p(t')$ is the displacement vector of polymers. In this case, the viscoelastic stress behaves elastically. In the limit that τ_B, $\tau_S \to \infty$, thus, the viscoelastic model reduces to the gel model.[10,35]

It is reasonable to assume that the motion of polymer $\vec{v}_p$ is faster than the relaxation of viscoelastic stresses in the early stage of phase separation (eq 22). Thus, the time development equation of the concentration field around the initial concentration ϕ_0, $\delta\phi(\vec{r}, t) = \phi(\vec{r}, t) - \phi_0$, is approximated up to the second order in $\delta\phi$ as

$$\frac{\partial \delta\phi}{\partial t} \approx \vec{\nabla}^2 \{ (a(\phi_0, \chi) - C' \vec{\nabla}^2) \delta\phi + b(\phi_0, \chi) \delta\phi^2 + O(\delta\phi^3) \} \quad (23)$$

$$a(\phi_0, \chi) = \frac{1}{\zeta} \Big[k_B T \Big\{ \phi_0(1-\phi_0) + \Big(\frac{1}{N_p} - 1 \Big) \phi_0 (1-\phi_0)^2 - 2\chi \phi_0^2 (1-\phi)^2 \Big\} + (1-\phi_0)^2 \Big\{ G_B(\phi_0) + \Big(2 - \frac{2}{d} \Big) G_S(\phi_0) \Big\} \Big] \quad (24)$$

$$C' = C \phi_0^2 (1-\phi_0)^2 / \zeta \quad (25)$$

Here the relation $\delta\phi \approx -\phi_0 \vec{\nabla} \cdot \vec{u}_p$ is used.

The first term of the right-hand side (rhs) of eq 23 corresponds to the Cahn's linearized theory. The coefficient of this term includes the mechanical stresses in the form of the longitudinal modulus, $G_B(\phi_0) + (2 - 2/d) G_S(\phi_0)$. This appearance of the longitudinal modulus is natural since the spinodal decomposition is described by the superposition of the plane waves. Since the spinodal line is effectively shifted to the low temperature due to the bulk and the shear stresses in the early stage of phase separation, spinodal decomposition is suppressed and the phase separation proceeds in the nucleation-growth-type mechanism.

Here we consider how the viscoelasticity affects the selection of the domain morphology. The second term of the rhs of eq 23 is the lowest even order of $\delta\phi$ and plays an important role in determining which phase becomes a majority one. Generally, the condition $[b(\phi_0, \chi) = 0]$ gives the composition symmetry line, where the two phases has the equal volume, or the pattern is symmetric against the exchange of the phase of $\delta\phi > 0$ with that of $\delta\phi < 0$. If we assume that the nucleated droplet has a spherical shape, the coefficient of the second term is given by

$$b(\phi_0, \chi) = -\frac{k_B T}{\zeta} \Big\{ \frac{3}{2} \Big(1 - \frac{1}{N_p} \Big) \phi_0^2 + \Big(\frac{2}{N_p} - 1 \Big) \phi_0 - \frac{1}{2N_p} - 2\chi \phi_0 (1-\phi_0)(2\phi_0 - 1) \Big\} + \frac{1}{\zeta} (1-\phi_0) \Big\{ \frac{(1-3\phi_0)}{2\phi_0} G_B(\phi_0) + (1-\phi_0) \frac{\partial}{\partial \phi} G_B(\phi_0) \Big\} \quad (26)$$

Because the shear mode is effectively decoupled to the bulk stress and does not affect the diagonal part of the osmotic tensor for a spherical domain, the contribution of the shear stress can be neglected in calculating eq 26. Of course, we must consider the contribution of the shear stress for the other shapes of droplets. For example, the coefficient depends on $G_B + {}^1/_3 G_S$ for a cylindrical domain, while it depends on $G_B + {}^4/_3 G_S$ for a lamellar structure. The possibility of the anisotropic shape of nuclei will be considered later. For the analytical argument, however, we assume a spherical shape for simplicity. For this case, the term $(\partial/\partial\phi) G_B(\phi_0)$ determines the composition symmetry line. It can be regarded as a measure of the dynamical asymmetry. Thus, we conclude that the composition symmetry line shifts toward the solvent-rich side and the solvent-rich phase nucleates selectively even when this phase is a majority one.

In connection to this, it should be noted that Onuki studied the effects of shear stress on nucleation of a spherical polymer-rich droplet in a metastable semidilute polymer solution.[36] The growth process of the droplet was mainly studied, and it was demonstrated that the viscoelastic shear stress decelerates the droplet growth. In the above, we do not take the shear stress into account, provided that the droplets are spherical. For a case of the nucleation and growth of droplets, however, this assumption is not so easily justified by analytical arguments; thus, we cannot deny the possibility that the shear stress may affect which phase is nucleated. To answer this difficult question, we make numerical simulations of phase separation with only shear stress of a step-function form (case f) instead of the form of eq 15. We confirm that even for this case the solvent-rich phase is selectively nucleated. This leads us to a conclusion that the shear stress does not affect the selectivity of the phase. However, the strong dependence of the shear modulus on the concentration $(\partial/\partial\phi) G_S(\phi_0)$ may affect the shape of nucleated domains although we assume that they are spherical in the above discussion just for simplicity. For example, when we set $G_S = (d/2) G_B (\propto \Theta(\phi - \phi_0))$ (case g), the nucleated domain is found to be not spherical but rather oblate. This anisotropic shape of domains may be realized to reduce the total deformation energy of the matrix phase. Note that these anisotropic nuclei are made of a solvent-rich phase even for this case. This problem may be related to the anisotropic crack pattern formation in an elastic medium such as gels. Further analytical and numerical studies are necessary for clarifying how bulk and shear stresses affect the early stage of viscoelastic phase separation.

In the late stage of phase separation, both mechanical stresses relax and we can neglect the viscoelastic contributions there. The coefficients of the first and second-order terms become

$$a' = \frac{k_B T}{\zeta}\phi_0(1-\phi_0)\left\{\frac{1}{N_P} + \left(1 - \frac{1}{N_p}\right)\phi_0 - 2\chi\phi_0(1-\phi_0)\right\} \quad (27)$$

$$b' = \frac{k_B T}{\zeta}\left\{\frac{1}{2N_p} + \left(1 - \frac{2}{N_P}\right)\phi_0 + \frac{3}{2}\left(\frac{1}{N_P} - 1\right)\phi_0^2 - 2\chi\phi_0(1-\phi_0)(1-2\phi_0)\right\} \quad (28)$$

Figure 1 schematically shows the effective phase diagrams for the early stage (gel regime) and the late stage (fluid regime) of phase separation. The phase diagram of the former is determined by eqs 24 and 26, while that of the latter is determined by eqs 27 and 28, respectively. If the system is quenched to the region (B) between the two lines determined by (eq 26) [$b(\phi_0,\chi) = 0$] and (eq 28) [$b'(\phi_0,\chi) = 0$], the polymer-rich phase changes from a majority phase to a minority one with time. Thus, the phase inversion takes place for such a case. The moving droplet phase and the spongelike phase may be observed in regions A and C, respectively.[6]

V. Results and Discussion

A. Time Evolution of Domain Patterns. First we show how phase separation proceeds in three dimensions. Figure 2 shows the pattern evolution of phase separation with both bulk and shear stresses (case a). The images represent the interfaces separating two phases. The darker and brighter sides of the interface correspond to a polymer-rich and solvent-rich phase, respectively. Namely, the darker droplets are the solvent-rich phase, while the brighter network structure is the polymer-rich one.

In Figure 2, phase inversion is clearly observed. The solvent-rich phase nucleates after a frozen period despite this phase is thermodynamically a majority one. Then, these droplets grow in size, and at the same time, the polymer-rich phase shrinks as in the volume-shrinking phase transition of gels. The polymer-rich phase decreases its volume fraction, keeping the connectivity. As a result, the well-developed continuous networklike structure of the polymer-rich phase is formed even though it is thermodynamically a minority phase. In the late stage, the viscoelastic stresses relax, and this networklike structure becomes unstable and breaks up into polymer-rich droplets due to the hydrodynamic tube instability.[6,9,10]

The simulation reproduces the basic features of our experimental observation.[4,5] The pattern evolution in 3D simulations is essentially the same as that of our previous 2D simulations.[21] Reflecting the difference in the dimensionality, however, both phases are continuous even for networklike morphology for 3D. In other words, the networklike structure is a bicontinuous one. We can intentionally produce the networklike structure of a minority phase. Since the viscoelastic properties of a system is dominated by the connectivity of the more viscoelastic phase, the networklike structure transiently formed during viscoelastic phase separation should be much more viscoelastic than the final droplet structure. This point is very important for the industrial applications.

We also simulate other cases to reveal the roles of each stress by comparing the results. Figures 3−6 show the simulated pattern evolutions for phase separation with no stresses (b), with only shear stress (c), with only bulk stress (d), and with both bulk and shear stresses having a longer shear relaxation time (e), respectively (see Table 1). The volume fraction is the same for all the cases. Note that the simulation without any stresses (case b) corresponds to usual phase separation in a fluid model (model H). For this case, the well-known behavior is observed: The droplets of a minority phase (a

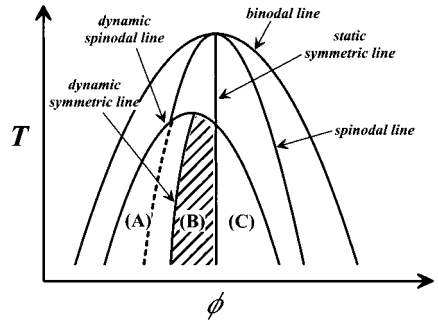

Figure 1. Schematic phase diagram of a dynamically asymmetric mixture. Within a shaded region (B), phase inversion should occur during phase separation.

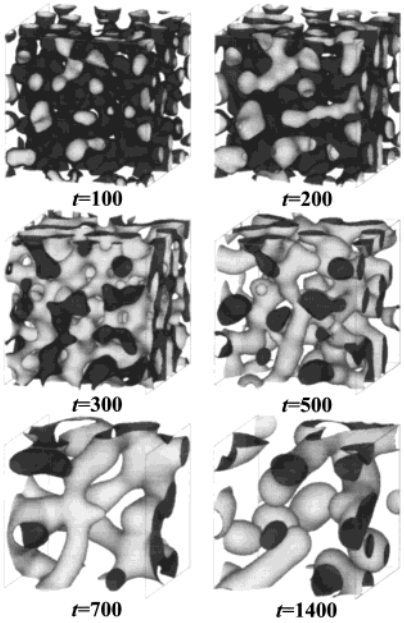

Figure 2. Simulated pattern evolution of phase separation with both bulk and shear stresses (case a). The light-gray side of the interface corresponds to the polymer-rich phase, while its dark-gray side corresponds to the solvent-rich phase.

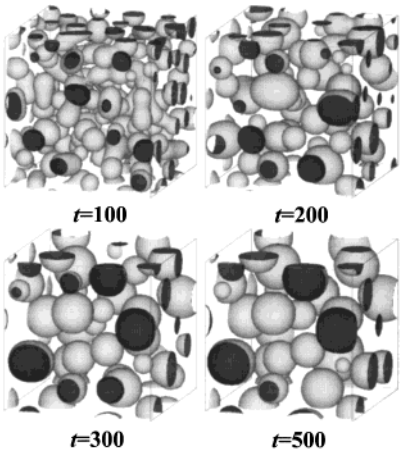

Figure 3. Simulated pattern evolution of phase separation without any mechanical stresses (case b).

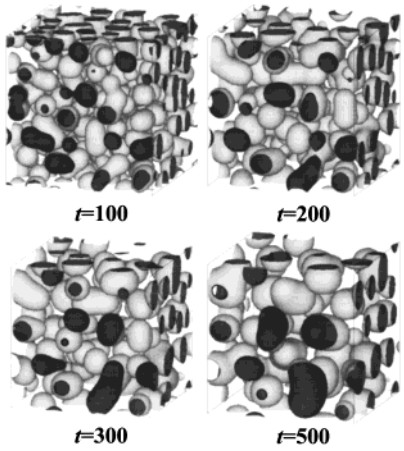

Figure 4. Simulated pattern evolution of phase separation with only shear stress (case c).

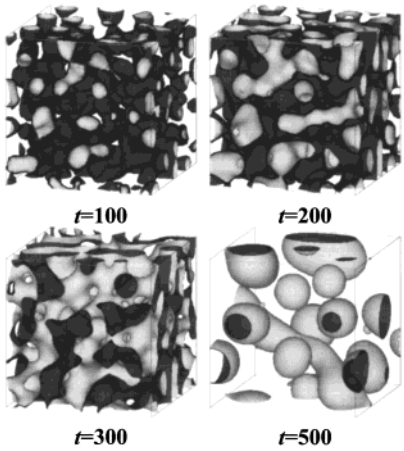

Figure 5. Simulated pattern evolution of phase separation with only bulk stress (case d).

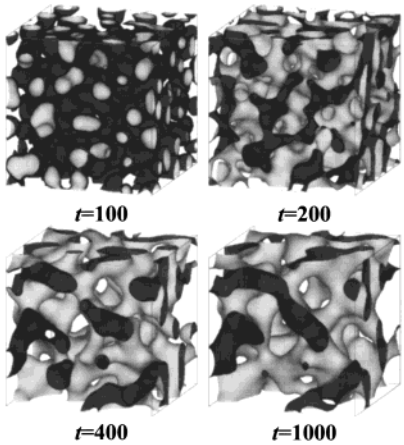

Figure 6. Simulated pattern evolution of phase separation with both bulk and shear stresses (case e). The relaxation time of shear stress is longer than that of case a.

polymer-rich phase) emerge just after the temperature quench and the droplets grow in time by the Lifshitz–Slyozov mechanism[37] and/or the coalescence mechanism.[38] Although the behavior of case c is essentially the same as that of case b, the coarsening rate of case c is a bit slower than that of case b (see Figure 11), because of the higher viscosity of a polymer-rich phase. A larger number of noncircular droplets are observed in case c than in case b. This is due to the fact that the shear stress slows down the shape-relaxation process.

In case d, on the other hand, the solvent-rich phase nucleates and the polymer-rich phase shrinks as in gels. The early-stage pattern evolution in case d is quite similar to that in case a. However, there is a large difference in the late stage between them: In case d, the networklike structure breaks up and the polymer-rich phase becomes spherical at the time when the volume shrinking is finished, while in case a the network structure keeps existing even after that time. Accordingly, the well-developed networklike structure is never formed in case d.

The behavior of case e is also similar to that of case a in the early stage, as expected. However, the pattern relaxation from a network to a droplet structure after the volume shrinking is much more retarded even compared to that in case a because the relaxation time of the shear stress is longer for case e than for case a. The final morphological transition to a droplet structure is not observed in our simulations simply due to the limitation of the computational time. The late-stage patterns for case e resemble the scanning electron microscope (SEM) images of fibrillar structures observed in phase separation of polymer solution.[39] In relation to this, we note that the dynamical asymmetry, which is characterized by the difference in the viscoelastic properties between the two phases, may be much stronger in real polymer solutions than in our simulations.

The above simulation results for various cases clearly demonstrate the roles of bulk and shear stresses. The bulk stress is responsible for the selective nucleation of a solvent-rich phase and the gellike volume shrinking behavior in the early stage, while the shear stress is responsible for the formation of the well-developed networklike bicontinuous structure. In the next section, we analyze how the osmotic, bulk, and shear stresses develop in time.

B. Temporal Change in Mechanical and Osmotic Forces and Their Roles. Figure 7 shows the temporal changes in the averaged magnitudes per lattice of the three types of forces, namely, the thermodynamic force $\vec{F}_\phi = -\vec{\nabla} \cdot \boldsymbol{\Pi}$, the bulk mechanical force $\vec{F}_B = -\vec{\nabla} \cdot \boldsymbol{\sigma}_B$, and the shear mechanical force $\vec{F}_S = -\vec{\nabla} \cdot \boldsymbol{\sigma}_S$ for case a.

After the temperature quench, the amplitude of the thermodynamic force increases and the bulk mechanical force follows it.[40] The thermodynamic and the bulk mechanical forces have their peaks almost at the same time $t \sim 340$. As will be shown in the next section, the volume shrinking has finished at this time. Both forces are closely related to the divergence of the velocity fields of polymer, $\vec{\nabla} \cdot \vec{v}_p$. The thermodynamic osmotic force causes the diffusional motion of polymer, and this motion induces the bulk stress. This is why the bulk force follows the osmotic force. Note that even if we use the larger value of G_B, the bulk stress can never exceed the osmotic one. These two forces have the opposite directions with each other, and thus they are mostly canceled out. As a result, the initial growth of concentration fluctuations, which is characteristic of usual spinodal decomposition, is significantly suppressed. The shear stress force has a peak at a time $t \sim 410$, retarded from those of the osmotic and the bulk forces by $\Delta t \sim 70$. The networklike structure begins to break up at this time $t \sim 410$. The degree of this retardation is dependent upon the relaxation time of the shear stress. The larger the shear relaxation time is, the longer the lifetime of the networklike structure is. In the networklike struc-

Table 1. ϕ Dependences of Moduli and Relaxation Times of Both Bulk and Shear Stresses Used in Simulations and Their Roles in the Early and Late Stage of Phase separation

case	$G_B(\phi)$	$\tau_B(\phi)$	$G_S(\phi)$	$\tau_S(\phi)$	phase inversion	morphology of droplets	networklike structure
a	$5.0\Theta(\phi-\phi_0)$	$10.0\phi^2$	$0.2\phi^2$	$10.0\phi^2$	o	spherical	o
b					×	(*polymer-rich droplets*)	×
c			$0.2\phi^2$	$50.0\phi^2$	×	(*polymer-rich droplets*)	×
d	$5.0\Theta(\phi-\phi_0)$	$10.0\phi^2$			o	spherical	×
e	$5.0\Theta(\phi-\phi_0)$	$10.0\phi^2$	$0.2\phi^2$	$50.0\phi^2$	o	spherical	o
f			$7.5\Theta(\phi-\phi_0)$	$10.0\phi^2$	×	(*polymer-rich droplets*)	(*numerically unstable*)
g	$5.0\Theta(\phi-\phi_0)$	$10.0\phi^2$	$7.5\Theta(\phi-\phi_0)$	$10.0\phi^2$	o	oblate	(*numerically unstable*)

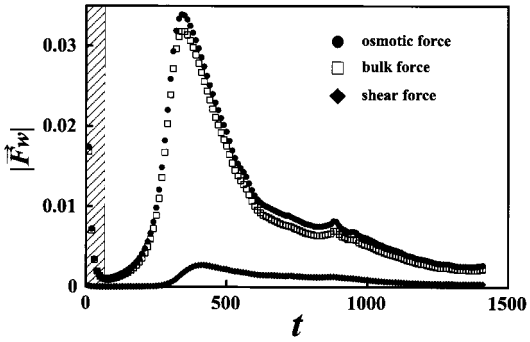

Figure 7. Temporal change in osmotic, bulk, and shear forces for case a.

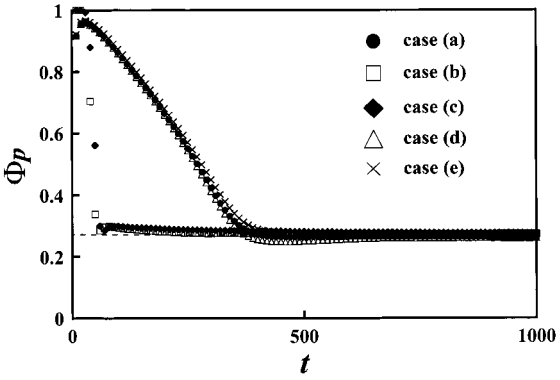

Figure 8. Temporal change in the volume fraction of the polymer-rich phase for cases a−e.

ture, the interface force, which is included in the off-diagonal part of the osmotic tensor, and the shear mechanical force are balanced as

$$\partial_i\left[C\left\{\partial_i\phi\partial_j\phi-\frac{1}{d}(\partial_l\phi)(\partial_l\phi)\delta_{ij}\right\}-\sigma_{Sij}\right]=0 \qquad (29)$$

The structure of the asymmetric fibrillar pattern is determined by this force balance condition.[9] We believe that the contribution of the osmotic stress (interface force) may be negligible in pattern selection for the elastic-force dominant regime. There are small peaks in the curves of the osmotic and bulk forces around $t \sim 800$. These peaks may reflect the morphological change from a network to a droplet structure. However, such peaks are not observed in our previous 2D simulations. Thus, further careful studies are required to clarify this point.

C. Composition Change during Phase Separation. Figure 8 shows the temporal change in the volume fraction for cases a−e. We assign the region with $\phi > 0.28$ to the polymer-rich phase. For cases without the bulk stress (b and c), the volume fraction almost reaches the final value of 0.245 soon after the temperature quench. On the other hand, they approach to the final

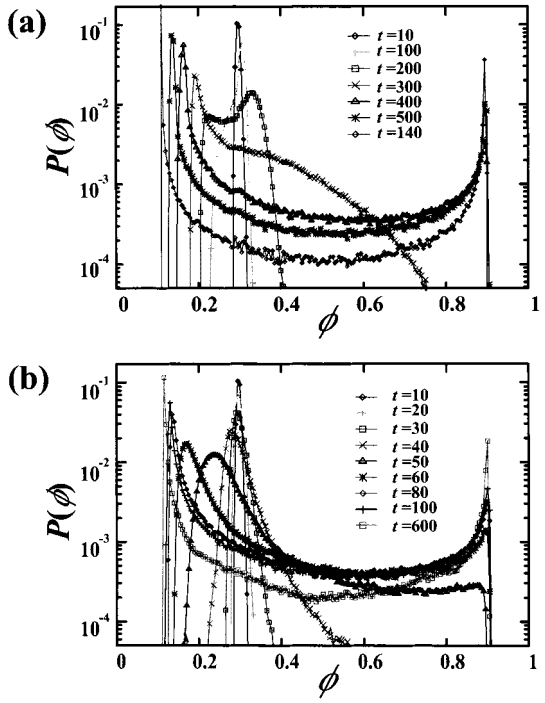

Figure 9. Temporal change in the concentration distribution function for cases a (a) and b (b).

value gradually for the case with bulk stress (a, d, and e). Note that the volume relaxation time strongly depends on the bulk relaxation time τ_B and is almost independent of the bulk modulus G_B. This is checked by our simulations, which are not presented here.

The effective osmotic pressure is given by[9]

$$\pi^{eff}(t) \approx \left(\phi\frac{\partial f_{FH}}{\partial\phi}-f_{FH}\right)+G_B\frac{\phi-\phi_0}{\phi_0}\exp(-t/\tau_B) \qquad (30)$$

Because the final equilibrium volume fraction is determined by χ and N_p in our model and does not depend on the viscoelastic parameters, all the studied cases, a−e, have the same equilibrium volume fraction of ∼0.245. The volume fraction during the volume shrinking at a time t is almost equal to that determined by the effective osmotic pressure (see eq 30). The longer the bulk relaxation time is, the more slowly the volume fraction approaches to the final value. It should be stressed here that shear stress never affects the kinetics of volume shrinking.

We also study the concentration change in viscoelastic phase separation by analyzing the concentration distribution function. Figure 9 shows the temporal change in the concentration distribution function for cases a and b. Figure 8 corresponds to the time dependence of the volume fraction of the region $\phi > 0.28$. For case a, the width of the concentration distribution increases much

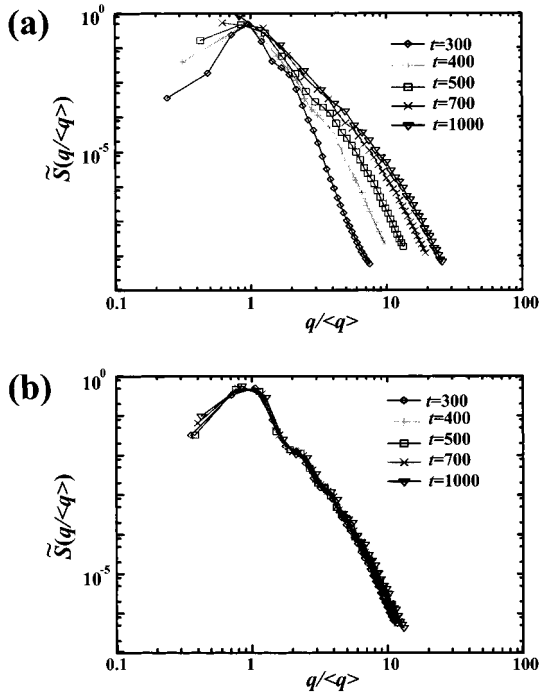

Figure 10. Time evolution of the scaled scattering function of cases a (a) and b (b).

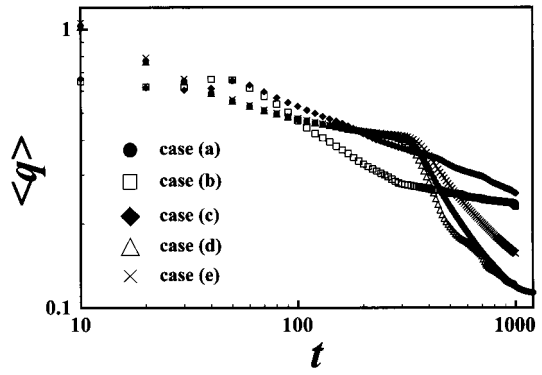

Figure 11. Temporal change of the characteristic wavenumber for cases a−e.

more slowly in the early stage than for case b since the growth of the concentration fluctuations are significantly suppressed for case a. Then the peak which corresponds to the solvent-rich droplets appears and grows, while the peak which is located around the initial concentration decays and disappears. These behaviors reflect the selective nucleation of the thermodynamically majority phase and the gellike volume shrinking. At $t \sim 300$, the volume fraction of the polymer-rich phase is nearly 50%, and the structure apparently looks similar to the usual bicontinuous phase separation. It should be noted, however, that the concentration distribution function is quite asymmetric, which is markedly different from usual bicontinuous phase separation. At $t \sim 340$ when the volume shrinking stops, the two peaks are located at $\phi_e \approx 0.1$ and 0.9, which correspond to the equilibrium concentrations. Further change in the concentration distribution is not observed for case a. For case b, on the other hand, a peak of the polymer-rich phase first appears at the final equilibrium concentration of the polymer-rich phase, $\phi_e \approx 0.9$. Although the final shapes of the histogram of cases a and b are, of course, the same as each other, their kinetic processes are very different. It is evident that this difference is caused by the bulk viscoelastic stress (see section IV).

D. Temporal Change in the Scattering Function. Figure 10 demonstrates the evolution of the scaled scattering function for viscoelastic phase separation (case a) and normal phase separation (case b). The scaled scattering function $\tilde{S}(q,t)$ is calculated by using 3D Fourier transformation as

$$S(q,t) = \frac{\int_{|\vec{q}'|=q}^{|\vec{q}'|=q+\mathrm{d}q} \mathrm{d}\vec{q}\, S(\vec{q},t)}{\int_{|\vec{q}'|=q}^{|\vec{q}'|=q+\mathrm{d}q} \mathrm{d}\vec{q}'} \tag{31}$$

$$\tilde{S}(q,t) = \frac{S(q,t)}{\int \mathrm{d}q'\, S(q',t)} \tag{32}$$

$$\langle q(t)\rangle = \frac{\int \mathrm{d}\vec{q}\ |\vec{q}|S(\vec{q},t)}{\int \mathrm{d}\vec{q}\ S(\vec{q},t)} \tag{33}$$

Figure 10b shows that for a fluid model (case b) the scaled scattering function is time independent except for the small wavenumber region. For case a, on the other hand, it does not collapse onto a single master curve at all. This indicates that the self-similarity hypothesis and the dynamical scaling law (see eqs 34 and 35), which are known to hold for fluid-fluid phase separation, break down for viscoelastic phase separation. Note that the dynamical scaling law is expressed as

$$\tilde{S}(q,t) = \langle q(t)\rangle^{-d} F(q/\langle q(t)\rangle) \tag{34}$$

$$\langle q(t)\rangle \propto t^{-\beta} \tag{35}$$

where F is a scaling function.

We demonstrate the temporal changes in the characteristic wavenumber calculated by eq 33 in Figure 11. The growth exponent β in the late stage of viscoelastic phase separation (case a) is about 0.27. However, since the dynamic scaling relation (eq 34) does not hold in this case and the exponent depends on the viscoelastic parameters (especially, the relaxation time of the shear stress, τ_S), it is not meaningful to discuss the value of the exponent.

For cases a and d, in which phase inversion occurs, the characteristic wavenumber suddenly decreases at the time of phase inversion. This time coincides with the end of the volume shrinking, which indicates that the drastic change of the domain pattern, i.e., phase inversion, takes place just after the completion of the volume shrinking. The characteristic length right after the volume shrinking is primarily determined by the spatial distribution of the solvent-rich droplets nucleated in the early stage. If the bulk stress suppresses concentration fluctuations more strongly, the probability of the nucleation of solvent-rich droplets becomes smaller. Thus, the distance between the solvent-rich droplets, which is one of the characteristic lengths of phase separation, should become larger.

Finally, it should be noted that pattern evolution should in principle become self-similar in the very late (asymptotic) regime, where phase separation should be described by a fluid model (model H). However, this regime is rather difficult to observe either experimentally or numerically.

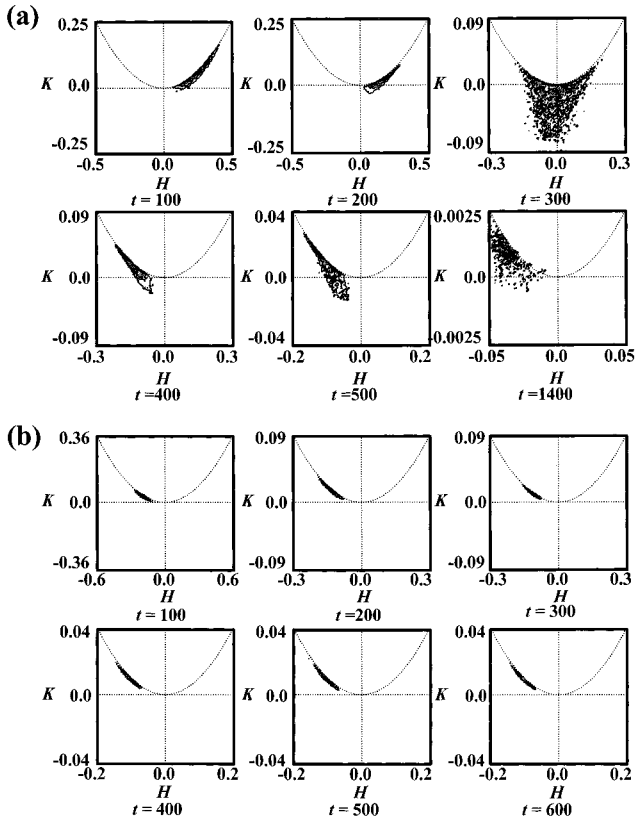

Figure 12. Temporal change in the distribution of mean and Gaussian curvatures of the interface for cases a (a) and b (b).

E. Topological Change of Domain Morphology during Phase Separation. 1. Curvature Analysis. We also analyze the mean and Gaussian curvatures of the interface to study the topological characteristics of the phase-separated structure.[41−44] To do so, we first define the interface as follows. We define Φ at each lattice point (α,β,γ) so that $\Phi = 1$ for $\phi \geq \phi_0$ while $\Phi = 0$ for $\phi < \phi_0$. Then we introduce the interface function $d(\alpha,\beta,\gamma)$ so that $d = 1$ when $\Phi(\alpha,\beta,\gamma) = 1$ and $\Pi_{l=\pm1,0}\Pi_{m=\pm1,0}\Pi_{n=\pm1,0}\Phi(\alpha + l, \beta + m, \gamma + n) = 0$; otherwise, $d = 0$. Thus, the interface Σ is defined by a group of points, where $d(\alpha,\beta,\gamma) = 1$. Then we calculate at all the lattice points the quantities

$$\tilde{H} = \partial_i n_i/2 \tag{36}$$

$$\tilde{K} = \{(\partial_k n_k)^2 - (\partial_i n_j)(\partial_i n_i)\}/2 \tag{37}$$

where $\vec{n} = \vec{\nabla}\phi/|\vec{\nabla}\phi|$. These quantities $\tilde{H}$ and $\tilde{K}$ on the interface Σ can be regarded as the mean and Gaussian curvatures H and K, respectively. Then the average mean and Gaussian curvatures, $\langle H\rangle$ and $\langle K\rangle$, are, respectively, calculated as

$$\langle H\rangle = \sum_{\alpha,\beta,\gamma} \tilde{H}(\alpha,\beta,\gamma)d(\alpha,\beta,\gamma)/\sum_{\alpha,\beta,\gamma} d(\alpha,\beta,\gamma) \tag{38}$$

$$\langle K\rangle = \sum_{\alpha,\beta,\gamma} \tilde{K}(\alpha,\beta,\gamma)d(\alpha,\beta,\gamma)/\sum_{\alpha,\beta,\gamma} d(\alpha,\beta,\gamma) \tag{39}$$

In Figure 12, the temporal changes of the distribution of the mean curvature H and the Gaussian curvature K in the $H-K$ plane are presented for cases a and b. In Figure 12b, the distribution of the curvatures is almost localized on the parabolic curve $K = H^2(H < 0)$, which means that the two principal curvatures have the same value at all points on the interface. That is, the polymer-rich domains have a spherical shape. The absolute average value of H, $|\langle H\rangle|$, decreases with time. Since the inverse of the absolute value of the mean curvature coincides with the average radius of a spherical droplet, the width of the curvature distribution corresponds to the size distribution of droplets in a real space. Thus, the shift of the distribution to the smaller absolute value reflects the coarsening process of the droplet structure.

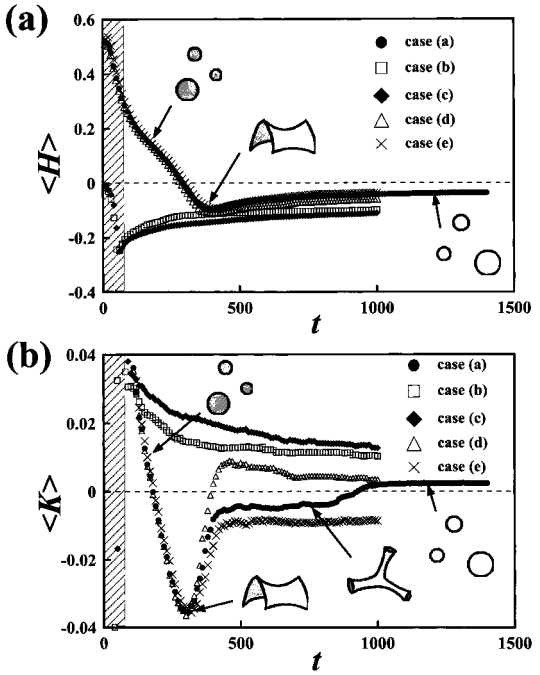

Figure 13. Temporal changes in the averaged mean (a) and Gaussian curvatures (b) of the interface.

The behavior of case a is, on the other hand, quite different from that of case b. The (H,K) distribution is localized on the curve $K = H^2(H > 0)$ in the early stage of phase separation, which means that the solvent-rich spherical droplets are formed. Next, the distribution shifts to the region $H \sim 0$, $K < 0$ at $t \sim 300$. The distribution pattern at this time is similar to that of a bicontinuous structure of symmetric spinodal decomposition obtained experimentally by Jinnai et al.[41] Note that the volume fraction of the polymer-rich phase is nearly 50% in their experiments and also at $t \sim 300$ in our simulation of case a. As time goes on, the (H,K) distribution moves toward the curve $K = H^2(H < 0)$.

In Figure 13 the temporal changes in the averaged mean and Gaussian curvatures are presented for cases a−e. Since our method to calculate the curvatures requires the sharp interface dividing the two phases, we cannot analyze the behaviors of the early stage (the shaded region in Figure 13) properly. For cases without bulk stress [(b) and (c)], the polymer-rich droplet structure, which has negative $\langle H\rangle$ and positive $\langle K\rangle$, is formed and then coarsens with time. Reflecting this coarsening process, their absolute values gradually decrease with time. For cases with bulk stress (a, d, and e), on the other hand, the averaged mean curvature has a positive value in contrast to the above cases (b and c). Then, its sign becomes negative. This change in the sign of the averaged mean curvature reflects the phase inversion. On the other hand, the averaged Gaussian curvature changes its sign twice, namely, from positive

to negative and then from negative to positive, for cases a and d. The first change reflects the morphological change from the nucleated solvent-rich droplet structure, which is characterized by positive K, to the bicontinuous pattern with saddle-like structures, which is characterized by negative K. The second one reflects that this asymmetric bicontinuous structure breaks up and transforms into the polymer-rich droplet structure, which is characterized by positive K. Since the relaxation time of the shear stress is long for case e, the breakup of the network structure and the resulting morphological change to the droplet structure are not observed within the computation time. So, the averaged Gaussian curvature remains negative in the late stage and does not yet change its sign for case e.

Figure 13 shows that the time when the averaged Gaussian curvature has the minimum value is almost the same as the time when the averaged mean curvature changes its sign at $t \sim 300$. This time also coincides with the time when the volume fraction (see section VC) is nearly 50%. From the direct observation of Figure 2, the structure at this time is quite similar to the bicontinuous structure observed in normal phase separation and the sponge phase in microemulsions. As time goes on, the averaged mean curvature has the minimum value at $t \sim 340$. Then, it approaches to zero asymptotically, reflecting the decrease in the mean curvature due to the coarsening process in the late stage. This time $t \sim 340$ corresponds to the end of gellike volume shrinking of the polymer-rich phase.

Almost at the same time, the averaged Gaussian curvature enters into a plateau regime for cases with both stresses (cases a and e). This plateau is related to the formation of the network structure due to the shear stress, which is supported by the fact that the plateau is not observed for case d. Interestingly, it is shown for case e that although the absolute value of the averaged mean curvature decreases, the plateau is quite flat at $t > 400$. Note that this behavior is also observed in case a although it is not so pronounced. According to the Gauss−Bonnet theorem, the integrated value of the Gaussian curvature on the whole interface is topologically invariant. Namely, the integrated Gaussian curvature is not changed unless the events of the breakup of the network and/or the coagulation of droplets occur. However, the Gaussian curvature, which is shown here, is simply the averaged value. Thus, the behavior observed in case e does not necessarily mean that the structure coarsens without any topological change. Actually, the breakup of the network is observed even for $t > 400$. We speculate that almost no change in the averaged Gaussian curvature in the late stage results from the canceling out of the two competing effects, the breakup of a network structure into a droplet one and the decrease in the total amount of the interface due to the domain-shape relaxation driven by the interface tension. This point will be discussed in the next section.

As described above, when the volume shrinking stops, the structure is bicontinuous for case a. It is believed that for an ordinary dynamically symmetric system a bicontinuous structure is observed when the volume fraction of one of the separated phases is almost equal to that of the other. In such a structure, the averaged mean curvature $\langle H \rangle$ is nearly zero.[41] On the other hand, a very asymmetric bicontinuous structure, in which the averaged mean curvature has a nonzero value ($\langle H \rangle < 0$), can be observed for viscoelastic phase separation:

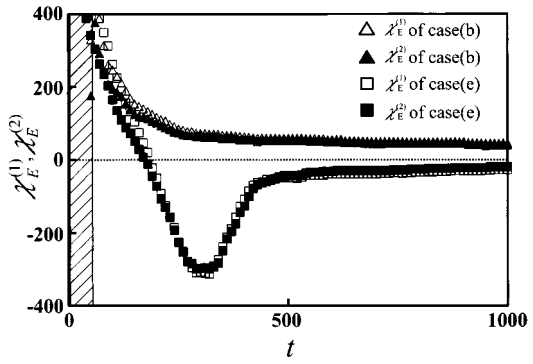

Figure 14. Temporal changes in the Euler characteristics for cases b and e by using two calculation methods (the integrated Gaussian curvature $\chi_E^{(1)}$ and the topological measure $\chi_E^{(2)}$).

For this structure, both phases are percolated even for a small volume fraction of a polymer-rich phase.

2. Analysis of the Euler Characteristic. Next we analyze the topological change during viscoelastic phase separation in terms of the Euler characteristic χ_E. Figure 14 shows the temporal changes in χ_E for normal phase separation (case b) and viscoelastic phase separation with a longer relaxation time of shear stress (case e). We calculate χ_E by two different methods. One is the integrated value of Gaussian curvatures over the whole interface Σ as

$$\chi_E^{(1)} = \frac{1}{2\pi} \int_\Sigma K \, dS = \frac{1}{2\pi} \sum_{\alpha,\beta,\gamma} \tilde{K}(\alpha,\beta,\gamma) d(\alpha,\beta,\gamma) \quad (40)$$

The other is the topological method: First we express the domain structure by polygons on the domain interface. Since we use the cubic lattice in this study, the interface is presented by squares. Then χ_E can be obtained as

$$\chi_E^{(2)} = F + V - E \quad (41)$$

where F, V, and E are the number of faces, vertexes, and edges of all polygons, respectively.[43] According to the Gauss-Bonnet theorem, $\chi_E^{(1)}$ should be equal to $\chi_E^{(2)}$. We confirm that the relation $\chi_E^{(1)} \cong \chi_E^{(2)}$ holds well in the late stage, which supports the validity of our analysis. The slight difference between $\chi_E^{(1)}$ and $\chi_E^{(2)}$ and in the early stage ($t < 300$) may stem from the uncertainty in the definition of the interface in calculating $\chi_E^{(1)}$.

For case b, χ_E monotonically decreases reflecting the decrease in the number of droplets. Note that for a droplet structure the number of droplets is given by $\chi_E/2$. For case e, on the other hand, the behavior of χ_E is similar to that of the averaged Gaussian curvature $\langle K \rangle$ (see Figure 13b). By definition, the time when the sign of χ_E becomes negative should coincide with that for the averaged Gaussian curvature. At $t \sim 300$, χ_E has the minimum value, and this large negative value of χ_E means that the domain structure is highly interconnected. Note that this time again corresponds to the time when $\langle K \rangle$ is minimal. However, the behavior of χ_E in the late stage of case e is different from that of $\langle K \rangle$. Namely, the value of χ_E becomes half from $t = 500$ to $t = 1000$ (see Figure 14), while the value of $\langle K \rangle$ of case e is almost constant, or it fluctuates within ~5% there. This strongly indicates that the topological feature of the networklike structure is changing with time, reflect-

ing the breakup of the polymer-rich network. This supports the discussion in the preceding section.

Finally, it may be worth noting that these topological features can hardly be obtained from the *q*-space analysis, as mentioned in section VD. The breakdown of the self-similarity is shown much more clearly by the topological analysis in real space than that by *q*-space analysis. Thus, we conclude that the curvature analysis and the analysis of the topological measure is quite powerful for characterizing the pattern evolution of viscoelastic phase separation.

VI. Conclusion

Viscoelastic phase separation is simulated in three dimensions. The results are basically consistent with what is observed in our 2D simulations.[21] The roles of bulk and shear stresses in 3D phase separation are found to be the same as those in 2D one, despite that the shear stress includes the dimensionality in its definition. The physical origin of a fibrillar pattern experimentally observed in a 3D phase-separated polymer solution is discussed. The bulk stress is directly coupled to the concentration diffusion. Thus, it induces the volume shrinking of the polymer-rich phase and the resulting phase inversion. The shear stress, on the other hand, plays a key role in the formation of a well-developed networklike pattern, whose structure is determined by the mechanical force balance condition. To elucidate the topological characteristics of patterns, we characterize the domain morphology by calculating the mean and Gaussian curvatures, their distributions, and the Euler characteristic, in addition to the conventional analysis in *q*-space. The topological analysis indicates that the network structure in viscoelastic phase separation essentially differs from the well-known bicontinuous structure ($\langle H \rangle \approx 0$) observed in a mixture of symmetric composition: It should be called an "asymmetric" bicontinuous structure ($\langle H \rangle \neq 0$).

We believe that the physical origin of bulk stress is due to the transient gel formation, which is universal to dynamically asymmetric mixtures.[8,45,46] This point needs further study.

Acknowledgment. This work was partially supported by a grand-in-aid from the Ministry of Education, Science, Culture, and Sports, Japan.

References and Notes

(1) Gunton, J. D.; San Miguel, M.; Sahni, P. In *Phase Transition and Critical Phenomena*; Domb, C.; Lebowitz, J. H.; Eds.; Academic: London, 1983.
(2) Hohenberg, P. C.; Halperin, B. I. *Rev. Mod. Phys.* **1976**, *49*, 435.
(3) See, e.g.: Bates, F. S.; Wiltzuis, P. *J. Chem. Phys.* **1989**, *91*, 3258.
(4) Tanaka, H. *Macromolecules* **1992**, *25*, 6377.
(5) Tanaka, H. *Phys. Rev. Lett.* **1993**, *71*, 3158.
(6) Tanaka, H. *J. Chem. Phys.* **1994**, *100*, 5253.
(7) Tanaka, H. *Phys. Rev. Lett.* **1996**, *76*, 787.
(8) Tanaka, H. *Phys. Rev. E* **1999**, *59*, 6842.
(9) Tanaka, H. *J. Phys.: Condens. Matter* **2000** *12*, R207.
(10) Tanaka, H. *Phys Rev. E* **1997** *56*, 4451.
(11) de Gennes, P. G. *J. Chem. Phys.* **1980**, *72*, 4756.
(12) Helfand, E.; Fredrickson, G. H. *Phys. Rev. Lett.* **1989** *62*, 2468.
(13) Onuki, A. *J. Phys. Soc. Jpn.* **1988**, *57*, 699.
(14) Milner, S. T. *Phys. Rev. E* **1993**, *48*, 3874.
(15) Doi, M.; Onuki, A. *J. Phys. II (Fr.)* **1992**, *2*, 1631.
(16) Onuki, A. *J. Non-Crystalline Solid* **1994** *172*−*174*, 1151. Onuki, A.; Taniguchi, T. *J. Chem. Phys.* **1997**, *106*, 5761.
(17) Kumaran, V.; Frederickson, G. H. *J. Chem. Phys.* **1996**, *105*, 8304.
(18) Sappelt, D.; Jäckle, J. *Europhys. Lett.* **1997**, *37*, 13. Sappelt, D.; Jäckle, J. *Physica A* **1997** *240*, 453. Sappelt, D.; Jäckle, J. *Polymer* **1998**, *39*, 5253.
(19) Ahluwalia, R. *Phys. Rev. E* **1999**, *59*, 263.
(20) Taniguchi, T.; Onuki, A. *Phys. Rev. Lett.* **1996**, *77*, 4910.
(21) Tanaka, H.; Araki, T. *Phys. Rev. Lett.* **1997**, *78*, 4966.
(22) de Gennes, P. G. *Macromolecules* **1976**, *9*, 584. de Gennes, P. G. *Macromolecules* **1976**, *9*, 597.
(23) Brochard, F.; de Gennes, P. G. *Macromolecules* **1977**, *10*, 1157. Brochard, F. *J. Phys. (Paris)* **1983**, *44*, 39.
(24) Sagui, C.; Piche, L.; Sahnoune, A.; Grant, M. *Phys. Rev. E* **1998**, *58*, 4654.
(25) Okuzono, T. *Phys. Rev. E* **1997**, *56*, 4416.
(26) Bhattacharya, A.; Mahanti, S. D.; Chakrabarti, A. *Phys. Rev. Lett.* **1998**, *80*, 333. Liu, H.; Bhattacharya, A.; Chakrabarti, A. *J. Chem. Phys.* **1999**, *111*, 11183.
(27) Tanaka, T.; Filmore, D. J. *J. Chem. Phys.* **1979**, *70*, 1214.
(28) Tanaka, H. *Prog. Theor. Phys. Suppl.* **1997**, *126*, 333.
(29) Muratov, C. B. *Phys. Rev. Lett.* **1998**, *81*, 3699.
(30) Doi, M.; Edwards, S. F. *The Theory of Polymer Dynamics*; Clarendon Press: Oxford, England, 1986.
(31) de Gennes, P. G. *Scaling Concepts in Polymer Physics*; Cornell University Press: New York, 1979.
(32) Rendell, R. W.; Ngai, K. L.; McKenna, G. B. *Macromolecules* **1987**, *20*, 2250.
(33) Shinozaiki, A.; Oono, Y. *Phys. Rev. E* **1993**, *48*, 2622.
(34) Tanaka, H.; Araki, T. *Phys. Rev. Lett.* **1998**, *81*, 389.
(35) Onuki, A.; Puri, S. *Phys. Rev. E Rapid Commun.* **1999**, *59*, R1331.
(36) Onuki, A. *J. Phys. II (Fr.)* **1992**, *2*, 1505.
(37) Lifshitz, I. M.; Slyozov, V. V. *J. Phys. Chem. Solids* **1961**, *19*, 35.
(38) Binder, K.; Stauffer, D. *Adv. Phys.* **1976**, *25*, 343.
(39) Aubert, J. H. *Macromolecules* **1990**, *23*, 1446.
(40) In the very early stage ($t < 50$), all these forces decrease. This is because we introduce the random concentration fluctuations as an initial condition. The very short wavelength components of the fluctuations relax even for the quench into the unstable region. Hereafter, thus, we neglect this time regime (the shaded region in Figure 7) in all analyses.
(41) See e.g. Jinnai, H.; Nishikawa, Y.; Hashimoto, T. *Phys. Rev. E* **1999**, *59*, R2554.
(42) White, W. R.; Wiltzius, P. *Phys. Rev. Lett.* **1995**, *75*, 3012.
(43) Aksimentiev, A.; Moorthi, K.; Holyst, R. *J. Chem. Phys.* **2000**, *112*, 6049.
(44) Sofonea, V.; Mecke, K. R. *Eur. Phys. J. B* **1999**, *8*, 99.
(45) Tanaka, H.; Araki, T. *Phys. Rev. Lett.* **2000**, *85*, 1338.
(46) Araki, T.; Tanaka, H. Unpublished results.

MA001569N